Supplementary information for "Optimal control of a quantum sensor: A fast algorithm based on an analytic solution"

Santiago Hernández-Gómez*[1,2], Federico Balducci[3,4,5], Giovanni Fasiolo[6], Paola Cappellaro[7], Nicole Fabbri[1,8], and Antonello Scardicchio[3,4]

[1]European Laboratory for Non-linear Spectroscopy (LENS), Università di Firenze, I-50019 Sesto Fiorentino, Italy
[2]Dipartimento di Fisica e Astronomia, Università di Firenze, I-50019, Sesto Fiorentino, Italy
[3]The Abdus Salam ICTP – Strada Costiera 11, 34151, Trieste, Italy
[4]INFN Sezione di Trieste – Via Valerio 2, 34127 Trieste, Italy
[5]SISSA – via Bonomea 265, 34136, Trieste, Italy
[6]Università degli studi di Trieste, Piazzale Europa 1, 34127, Trieste, Italy
[7]Department of Nuclear Science and Engineering, Department of Physics, Massachusetts Institute of Technology, Cambridge, MA 02139
[8]Istituto Nazionale di Ottica del Consiglio Nazionale delle Ricerche (CNR-INO), I-50019 Sesto Fiorentino, Italy

April 19, 2022

1 Definition of the sensitivity

In the main text, Eq. (4) introduced the sensitivity η as the minimum detectable signal for unit time in our experimental platform. To justify this statement, here we sketch a brief derivation using both a direct approach, and a more formal one through the Fisher information.

First, let us define η as the signal strength yielding a signal-to-noise ratio SRN = 1 for a total experiment time of 1 s. Following Ref. [1], the SNR for N independent experiments can be defined as

$$\mathrm{SNR} = \frac{\delta P(T,b)}{\sigma_N}, \tag{1}$$

where σ_N encompasses all the sources of error, and $\delta P(T,b)$ is the spin population difference between the cases with and without target signal: $\delta P(T,b) = P(T,b) - P(T,0)$. Now, the error can be shown to be of the form $\sigma_N \approx C^{-1}/\sqrt{N}$, with a dimensionless constant $C = O(1)$ depending on the experimental platform [1]. Also, using Eq. (1) of the main text, and assuming slope detection, one easily gets to

$$\delta P(T,b) \approx e^{-\chi(T)} \left| \sin\left(\varphi(T,b)\right) \frac{\partial \varphi(T,b)}{\partial b}\, b \right| = e^{-\chi(T)} |\varphi(T,b)|. \tag{2}$$

Thus, imposing SNR $\equiv 1$ one finds

$$1 = e^{-\chi(T)} |\varphi(T,b)| \frac{1}{C\sqrt{N}} \tag{3}$$

*hernandez@lens.unifi.it

and finally, using that one performs N experiments in 1 s in total,

$$\eta = \frac{e^{\chi(T)}}{|\varphi(T)/b|}\sqrt{T}, \tag{4}$$

with T being the time for a single experiment, and C set to unity. This is exactly Eq. (4) of the main text.

As anticipated above, the sensitivity can be defined also through the Fisher information and the Cramér-Rao bound. Specifically, we define η to be the minimum signal that can be distinguished from 0 in a total time of 1 s. Assuming that our estimator of the magnetic field b is unbiased, from the Cramér-Rao bound it must be

$$\Delta b \geq \frac{1}{\sqrt{F_N}}, \tag{5}$$

where F_N is the Fisher information associated with N measurements of the magnetic field strength b from an estimator x [2, 3]:

$$F_N = \sum_x \frac{1}{p_N(x|b)} \left(\frac{\partial p_N(x|b)}{\partial b}\right)^2. \tag{6}$$

In our case, since we detect the $|\pm\rangle$ states in a Ramsey interferometry experiment, it holds $p(\pm|b) = \mathrm{Tr}(\rho|\pm\rangle\langle\pm|)$ with

$$\rho = \begin{pmatrix} 1/2 & e^{-\chi(T)-i\varphi(T,b)/2}/2 \\ e^{-\chi(T)+i\varphi(T,b)/2}/2 & 1/2 \end{pmatrix}, \tag{7}$$

and thus

$$F = \frac{8\varphi^2(T,b)}{b^2} \frac{e^{-2\chi(T)}\sin^2\varphi(T,b)}{1-e^{-2\chi(T)}\cos^2\varphi(T,b)}. \tag{8}$$

Assuming slope detection, and for N repeated measurements,

$$F_N = N\frac{8\varphi^2(T,b)e^{-2\chi(T)}}{b^2}, \tag{9}$$

since the Fisher information is additive for independent trials. At this point, recalling that the N experiments have to be done in a total time of 1 s, and using the Cramér-Rao bound Eq. (5), one easily gets to Eq. (4), that is Eq. (4) of the main text.

2 Details on the experimental platform

The ground state of an NV center is a spin triplet $S = 1$, naturally suited for sensing magnetic fields via Zeeman effect. The NV electronic spin presents extremely long coherence times, of the order of milliseconds at room temperature [4], due to the protective environment provided by the diamond itself. The $S = 1$ electronic spin can be initialized into the $m_S = 0$ state by addressing the NV center with green light (532 nm). This is due to an excitation–decay process involving radiative (637 nm) and non-radiative decay routes, occurring with a probability that depends on the spin projection m_S. This same mechanism implies that the red photoluminescence intensity of the $m_S = 0$ state is higher than the one of $m_S = \pm 1$, hence enabling to optically readout the state of the system. In addition, the internal structure of the NV center removes the degeneracy between the $m_S = \pm 1$ states and the $m_S = 0$ state, imposing a zero-field-splitting of $D_g \simeq 2.87$ GHz. An external bias field, aligned with the spin quantization axis, removes the degeneracy between the $m_S = \pm 1$ states, allowing to individually address the $m_S = 0 \leftrightarrow m_S = +1$ transition using on-resonance microwave radiation. By using microwave pulses with a appropriate duration, amplitude and phase, it is possible to apply any kind of gate to the single two level system. Therefore, the two level system formed by the $m_S = 0$ ($|0\rangle$) and $m_S = +1$ ($|1\rangle$) states fulfills the requirements to be used as a qubit based magnetometer.

2.1 Characterization of the amplitude of the target signal

The target signal is delivered via a signal radio-frequency (RF) generator connected to the same wire, placed close to the diamond, that delivers the MW control field. We can control the amplitude of the target field by changing the output amplitude of the RF generator. However, the absolute value of the amplitude of the target field b has to be characterized in order to take into account the attenuation of the circuit, the emission efficacy of the wire (which depends on the RF frequency) and the distance between the wire and the NV defect. To achieve such characterization, as explained in the main text, we measure the spin dynamics for a CP sequence as a function of the sequence interpulse time, and we compare with the simulation to minimize the residuals using b as the only free parameter. By performing this measurements for different values of the RF generator output amplitude a_{RF}, we can extract a relation between a_{RF} (in [Vpp]) and the amplitude of the target magnetic field b (in [T]).

3 Additional test cases

In order to reinforce our results, we repeated the analysis presented in the main text for two different target signals. A monochromatic target signal that coincides with one of the NSD harmonics, and a 7-chromatic target signal that accentuates the difference between the generalized CP and the optimal solution.

3.1 Second test case: Monochromatic target signal

If we want to detect a monochromatic target signal $b(t)$, in most cases a Carr-Purcell CP sequence of equidistant pulses is the best way to increase the sensor's response to that target signal and filter out the noise. This is due to the quasi-monochromatic filter function associated with a CP sequence. Assuming that τ is the time between pulses, the filter function shows a peak centered at $\omega/2\pi = \frac{1}{2\tau}$. However, the filter function is not exactly monochromatic, it shows harmonics at $\omega/2\pi = \frac{1}{2(2\ell+1)\tau}$, with $\ell \in \{1, 2, ...\}$. Therefore, if the frequency associated with $b(t)$ is close to $\omega_{\mathrm{L}}/(2\ell+1)$, then a CP sequence will amplify the effect of both, the target signal and the noise, leading to not-optimal sensitivities.

Here we used the optimization algorithm described in the main text in order to obtain optimal sequences for this problem. In particular, we explored the case of a monochromatic signal with frequency $\nu_{\mathrm{mono}} = 39.29$ kHz, which is close enough to $\nu_{\mathrm{L}}/11$ so that the 5-th harmonic of the CP sequence coincides with the noise components. We used the same NSD $S(\omega)$ as in the three-chromatic case. The experimental values of $1/\eta$ are obtained from the measurement of $P(T, b)$ as a function of b. The results of $P(T, b)$ for one value of the sensing time T are shown in Fig. 1(a). The predicted values of the inverse sensitivity, together with their experimental values are shown in Fig. 1(b). Similarly to the case detailed in the main text, the optimal sequences improve the sensitivity of the quantum sensor, resulting in some cases to an inverse sensitivity that is close to a twice the one from the CP sequence. In the monochromatic case explored here, the sensitivity gets worse when increasing the sensing time beyond 100 μs. Instead the optimal solutions are able to improve the sensitivity even for times $T > 300$ μs. For $T \simeq 100$ μs, and longer sensing times, the optimized sequences achieve higher values of $1/\eta$ than the maximum value achieved by a CP sequence.

3.2 Third test case: 7-chromatic target signal

We have explored the case of a target signal with 7 frequency components, as specified in Fig. 2 (a-b). As in the main text, we used the optimization algorithm either to find the approximated spherical solution, or the solution using simulated annealing (SA) in order to minimize the sensitivity. The predicted values of the inverse sensitivity, together with their experimental

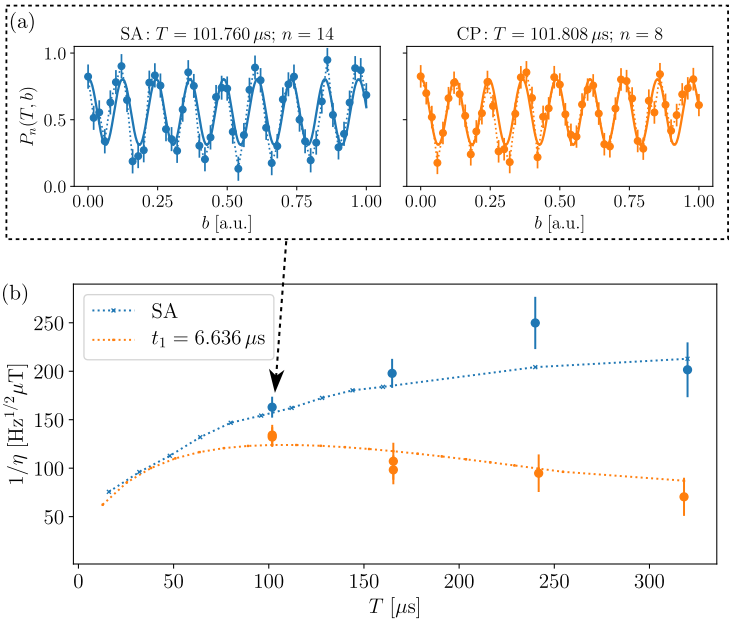

Figure 1: Results for the case of a monochromatic target signal. (a) Probability to remain in the state $|1\rangle$ as a function of b, for fixed sensing times T for an optimal DD sequence (blue), and for a CP sequence (orange). The values of the sensing time and of the number of pulses for both sequences are shown as titles of the plots. A cosine function is fitted (solid lines) to the experimental data (bullets with errorbars) in order to obtain $1/\eta$ (see main text). (b) Inverse sensitivity as a function of the sensing time T. Blue data corresponds to the optimized sequences obtained with simulated annealing (SA). Orange data corresponds to the CP sequences with $\tau = 12.726$ μs. We found a good agreement between the predicted values (dotted lines) and the experimental values (bullets with errorbars).

(a)

i	A_i	ν_i [MHz]	c_i
0	0.213919	0.420068	2.248311
1	0.130194	0.564180	0.451269
2	0.141141	0.226517	2.531370
3	0.031116	0.900518	2.715790
4	0.050013	0.756436	0.265970
5	0.320765	0.286164	5.786594
6	0.112853	0.366105	1.622823

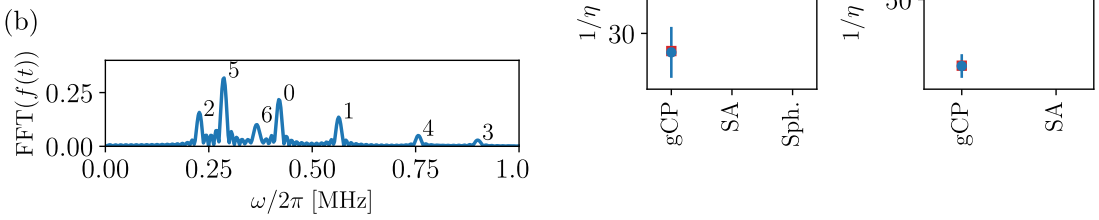

Figure 2: Results for the case of a target signal with seven frequency components. (a) Table to indicate the amplitude, frequency and phase of each component of the target signal $f(t) = \sum_{i=0}^{6} A_i \cos(2\pi\nu_i t + c_i)$. (b) Fast Fourier transform (FFT) of the target signal. (c) Inverse sensitivity for $T = 80$ μs and 160 μs. The predicted values (squares) and the experimental values (bullets with errorbars) show that the sequences obtained from the spherical solution (Sph.) or from the simulated annealing solution (SA) result in an improved sensitivity with respect to the generalized CP (gCP) sequences.

values are shown in Fig. 2(c). Similarly to the previous test cases, the optimal sequences improve the sensitivity of our quantum sensor. In this case, the sensitivity obtained with the optimal solutions almost 1/2, and 1/3 with respect to the generalized CP (gCP) sequence for $T = 80$ μs, and $T = 160$ μs, respectively.

References

[1] C. L. Degen, F. Reinhard, and P. Cappellaro, Rev. Mod. Phys. **89**, 035002 (2017).

[2] S. L. Braunstein and C. M. Caves, Phys. Rev. Lett. **72**, 3439 (1994).

[3] F. Poggiali, P. Cappellaro, and N. Fabbri, Phys. Rev. X **8**, 021059 (2018).

[4] N. Bar-Gill, L. M. Pham, A. Jarmola, D. Budker, and R. L. Walsworth, Nat. Comm. **4**, 1743 (2013).